Journal of Physiology (1989), **416**, *pp.* 93–110
With 12 text-figures
Printed in Great Britain

HETEROGENEOUS DISTRIBUTION OF FAST AND SLOW POTASSIUM CHANNELS IN MYELINATED RAT NERVE FIBRES

BY JOCHEN RÖPER AND JÜRGEN R. SCHWARZ

From the Physiologisches Institut, Universitätskrankenhaus Eppendorf, D-2000 Hamburg 20, FRG

(*Received 6 January 1989*)

SUMMARY

1. Potassium currents were measured in voltage-clamped single myelinated rat nerve fibres before and after paranodal demyelination with 0·2% pronase or 0·2% lysolecithin added to the external solution. Sodium currents were blocked by 300 nM-tetrodotoxin. For the purpose of comparison, intact frog nerve fibres were also investigated.

2. Our results suggest the existence of at least two distinct types of K^+ channels in the intact node of Ranvier, one with slow and another with fast gating kinetics, in the ratio 4:1.

3. In the rat nodal membrane, slow K^+ channels have voltage-dependent time constants of K^+ deactivation with $\tau_n = 68$ ms at $E = -105$ mV and $\tau_n = 26$ ms at $E = -150$ mV at 20 °C. The activation curve of the slow K^+ conductance is sigmoid with an inflexion point at -60 mV. This means that about 35% of the slow K^+ channels are in the open state at the resting potential of -77 mV. Slow K^+ channels could be blocked by 10 mM-tetraethylammonium chloride, but were insensitive to 4-aminopyridine.

4. After paranodal demyelination the ratio of fast to slow K^+ channels increased from 17 to 83%. As in the frog (Dubois, 1981*a*), the population of fast K^+ channels in the rat may consist of two different subgroups, both of which can be blocked by 4-aminopyridine.

5. Demyelination was accompanied by an increase in the capacity current which was used to estimate the exposed membrane area. The density of slow and fast K^+ channels was calculated from the quotient of the steady-state K^+ conductance to membrane area. The density of the slow K^+ channels is maximal in the nodal membrane and decreases to 1/31 in the internode. By contrast, the distribution of the fast K^+ channels differs, their density being maximal in the paranode and decreasing to one-sixth in the node and internode.

INTRODUCTION

The nodal membrane of mammalian myelinated nerve fibres has been shown to contain 'virtually no' (Chiu, Ritchie, Rogart & Stagg, 1979) or 'almost no' (Brismar, 1980) K^+ channels. In intact mammalian myelinated nerve therefore, the activation of voltage-dependent K^+ channels is not required for the repolarization phase of the

action potential (Sherratt, Bostock & Sears, 1980; Schwarz & Eikhof, 1987). However, there are several reports indicating that the mammalian node of Ranvier has a complex functional organization with a distribution of K^+ channels differing from that in amphibian nerve fibres (Koksis, Waxman, Hildebrand & Ruiz, 1982; Koksis & Waxman, 1987). Although the total K^+ conductance in the mammalian nodal membrane is small, it has been shown that a fraction of the nodal K^+ conductance is already activated at the normal resting potential (Binah & Palti, 1981; Brismar & Schwarz, 1985). Furthermore, K^+ channels are not confined to the nodal membrane. After acute paranodal (Chiu & Ritchie, 1981) and internodal demyelination (Chiu & Schwarz, 1987) as well as after chronic demyelination (Brismar, 1979), large K^+ currents were recorded indicating the existence of K^+ channels normally buried under the para- and internodal myelin.

Hints for a functional importance of all of these K^+ channels came from intra-axonal microelectrode recordings. Baker, Bostock, Grafe & Martius (1987) showed that a block of K^+ channels by TEA induces a decrease in accommodation and that a block by 4-AP elicits bursts of action potentials in rat spinal root fibres. Their results indicated the existence of different types of K^+ channels in mammalian nerve fibres as well as a different location along the axolemma.

In myelinated frog nerve fibres three different types of K^+ channels were distinguished by Dubois (1981*a*). In addition to two fast K^+ channels which were selectively blocked by 4-AP, there was a population of slow K^+ channels blocked by TEA. Recently, Grissmer (1986) showed that fast and slow K^+ channels are also present in the frog internode. He demonstrated that the total K^+ channel density decreased from the nodal to the internodal membrane to 1/20 and that the ratio of slow to fast K^+ channels was larger in the internode than in the node. Similar data do not exist for the mammalian nerve fibre. Therefore, we performed voltage clamp experiments to determine whether there are also different types of K^+ channels in rat nerve fibres and, if this is the case, to determine some of their properties, their distribution, and their density in the nodal and internodal membrane.

Part of this work has been published in abstract form (Schwarz & Röper, 1988).

METHODS

Single myelinated nerve fibres were isolated from the sciatic nerve of adult albino rats (300–400 g, Sprague–Dawley) and a node of Ranvier was voltage clamped at 20 °C (Nonner, 1969). The rats were killed by cerebral dislocation. A few experiments were also performed in single nerve fibres of the frog (*Rana esculenta*). The frogs were killed by decapitation. The dissection of mammalian and amphibian nerve fibres was similar to that described by Stämpfli & Hille (1976).

At the beginning of each experiment, the holding potential was adjusted to give a steady-state Na^+ inactivation (h_∞) of about 0·7. The internodes of the nerve fibre mounted in the experimental chamber were cut in both side pools and bathed in isotonic KCl solution. After a stabilization period of about 20 min, the node of Ranvier was superfused with isotonic KCl solution and the reversal potential was determined (E_K). The holding potential was determined from the value of E_K and found to be $E_H = -77 \pm 1$ mV (mean ± S.E.M., $n = 22$) in rat nerve fibres. This value agrees well with that of −80 mV, given by Chiu *et al.* (1979) and Brismar (1980), and that of −78 mV, given by Neumcke & Stämpfli (1982). The value $E_H = -77$ mV was used to calculate absolute membrane potentials in those fibres where E_H was unknown. In frog nerve fibres, E_H was assumed to be −70 mV (Stämpfli & Hille, 1976).

Membrane current was recorded as the voltage drop across the internodal resistance, R_{ED}, between the cut end of the internode in pool E and the axoplasmic point D at the node under investigation (Nonner, 1969). Values of R_{ED} were assumed to be 15 and 20 MΩ on the basis of unpublished data of B. Neumcke, J. R. Schwarz and R. Stämpfli in the rat ($14{\cdot}4 \pm 2{\cdot}4$ MΩ; $n = 13$) and in the frog ($20{\cdot}3 \pm 1{\cdot}8$ MΩ; $n = 11$), respectively.

Membrane currents were filtered with a passive Bessel-filter (10 or 40 kHz), converted to analog-to-digital with a sampling interval of 4·5 μs (8 bit) and stored on disc for further analysis by a microcomputer (LSI 11/23). Linear leakage and capacity current components were measured at hyperpolarizing pulses in Ringer solution. In order to obtain specific currents, these leakage and capacity currents were appropriately scaled, multiplied by −1 and subtracted from the total membrane currents. The leakage current was the same in both Ringer solution and isotonic KCl solution.

Analysis of K^+ and capacity currents: a least-squares fitting procedure was used as described by Schwarz & Eikhof (1987). Potassium tail currents were fitted with the sum of two exponentials:

$$I = I_s \exp(-t/\tau_s) + I_f \exp(-t/\tau_f).$$

The four adjustable parameters were τ_s and τ_f, the time constants of the slow and fast tail current components together with their respective amplitudes, I_s and I_f.

The time constant of K^+ activation during a depolarizing pulse was obtained from a fit of the equation:

$$I_K = I_{K'}(1 - \exp(-t/\tau_n))^a$$

where $I_{K'}$ is the steady-state K^+ current and τ_n the time constant of K^+ activation. The exponent 'a' was set equal to 3 in all fits.

The capacity current was measured on a negative pulse in Ringer solution. In intact fibres it consisted of only one fast component. After stretch or demyelination, a second slow component emerged. The charges, Q_f and Q_s, of the fast and slow capacity component were obtained from the integration of a double exponential fitted to the capacity current (Chiu & Ritchie, 1982). The membrane capacity was calculated from the charge, and the amplitude of the negative pulse. The mean values and standard error of the mean were calculated in the statistical evaluations.

The solutions used in the rat experiments were composed as follows: Ringer solution (in mM): NaCl, 154; $CaCl_2$, 2·2; KCl, 5·6. Isotonic KCl solution (in mM): KCl, 160; $CaCl_2$, 2·2. Axoplasmic solution (in mM): KCl, 155; NaCl, 5. The solutions used in the frog experiments were composed as follows: Ringer solution (in mM): NaCl, 110; $CaCl_2$, 2·0; KCl, 2·5. Isotonic KCl solution (in mM): KCl, 112; $CaCl_2$, 2·0. Axoplasmic solution (in mM): KCl, 112; NaCl, 5. All solutions contained 5 mM-Tris-HCl and the pH was adjusted to 7·3. In order to block Na^+ currents, 300 nM-tetrodotoxin (TTX) was added to the external solutions. Potassium currents were blocked by 1 mM-4-aminopyridine (4-AP), 10 mM-tetraethylammonium chloride (TEA) or 25 μM-capsaicin (from a 25 mM stock solution in ethanol) in the external solutions. All solutions were saturated with oxygen in the rat experiments.

RESULTS

Comparison of ionic currents in the rat and frog node of Ranvier

Single myelinated rat and frog nerve fibres were voltage clamped. Figure 1 shows the membrane currents of both species elicited by positive potential steps of increasing amplitude. As has already been described by Chiu *et al.* (1979) in the rabbit and by Brismar (1980) in the rat, mammalian myelinated nerve fibres exhibit only a small K^+ outward current, whereas large outward K^+ currents are present in the frog fibre. The differences in K^+ conductance also lead to different tail currents. Upon repolarization, there were only very small K^+ tail currents in the rat, whereas large K^+ tail currents occurred in the frog. Figure 1 shows that inward Na^+ currents are almost the same in both species. The slightly faster decay of the inward currents in the frog fibre may be due to the additive effect of Na^+ inactivation and K^+

activation. Recently it has been shown that the steady-state parameters and gating kinetics of Na^+ current activation and inactivation are almost identical in the rat and frog (Neumcke, Schwarz & Stämpfli, 1987).

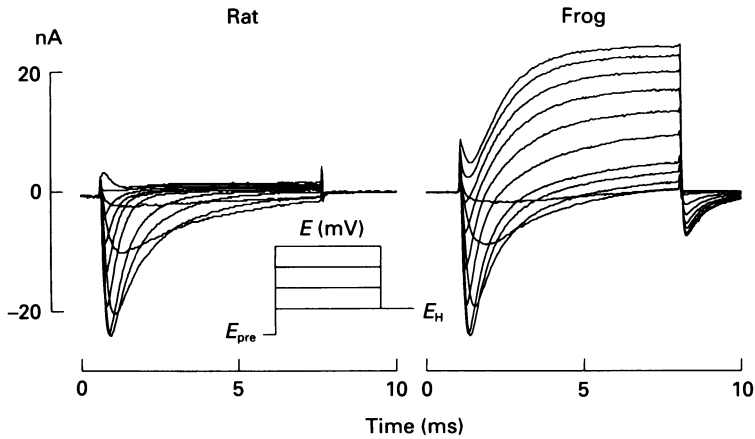

Fig. 1. Membrane currents in a rat and a frog nerve fibre elicited by depolarizing pulses from −45 to −15 mV in steps of 7·5 mV and from −15 to 75 mV in steps of 15 mV. Capacity and leakage currents have been subtracted. Each positive pulse was preceded by a 50 ms pulse to −125 mV (E_{pre}). E_H, holding potential of −75 mV in the rat and −70 mV in the frog. Tissue in Ringer solution.

In rat nerve fibres the outward K^+ current can be totally blocked by external TEA and axoplasmic CsCl (Schwarz & Eikhof, 1987). In the present experiments, the amplitude of this small K^+ outward current was $0{\cdot}51 \pm 0{\cdot}26$ nA ($n = 7$) at a depolarization to $E = 75$ mV. We interpret this value as being representative of the nodal K^+ current of the intact mammalian node of Ranvier. One indication of this is the very small membrane capacity of about 1·5 pF in all of these nerve fibres.

Properties of rat nodal K^+ currents

Further analysis of the K^+ currents shown in Fig. 1 was made in isotonic KCl solution + 300 nM-TTX. After exchange of Ringer for isotonic KCl solution, a small steady-state inward current occurred. This indicated the presence of open K^+ channels at the holding potential ($h_\infty = 0{\cdot}7$). Our experiments show that these K^+ currents present in intact rat nodes are characterized by slow gating kinetics and that they are deactivated at large negative membrane potentials. The nodal membrane was clamped at its holding potential in order to determine the voltage dependence of the steady-state slow K^+ conductance. In the experiment of Fig. 2*A*, a constant inward current of 2 nA was present at the holding potential of −75 mV. Hyperpolarizing pulses of increasing amplitude (see pulse protocol in Fig. 2*Ac*) elicited instantaneous inward currents which, after a delay of 5–10 ms, decayed with a potential-dependent time course to a constant inward current. In four fibres, the time constant of the decaying current was $67{\cdot}6 \pm 14{\cdot}9$ ms at −105 mV, $39{\cdot}7 \pm 8{\cdot}9$ ms at −120 mV, $31{\cdot}5 \pm 7{\cdot}6$ ms at −135 mV and $26{\cdot}1 \pm 5{\cdot}4$ ms at −150 mV. Positive pulses of increasing amplitude elicited outward currents (Fig. 2*Aa*). The outward currents decreased or increased to a steady state if the pulse potentials were $< E_K$

or $> E_K$. Addition of 10 mM-TEA to the external solution induced a potential-dependent block of the K^+ currents. The inward K^+ currents during negative pulses were abolished, whereas the K^+ currents at positive pulses were not completely blocked. The slow K^+ current, measured at $E = 25$ mV and shown in Fig. 2*Aa* as the

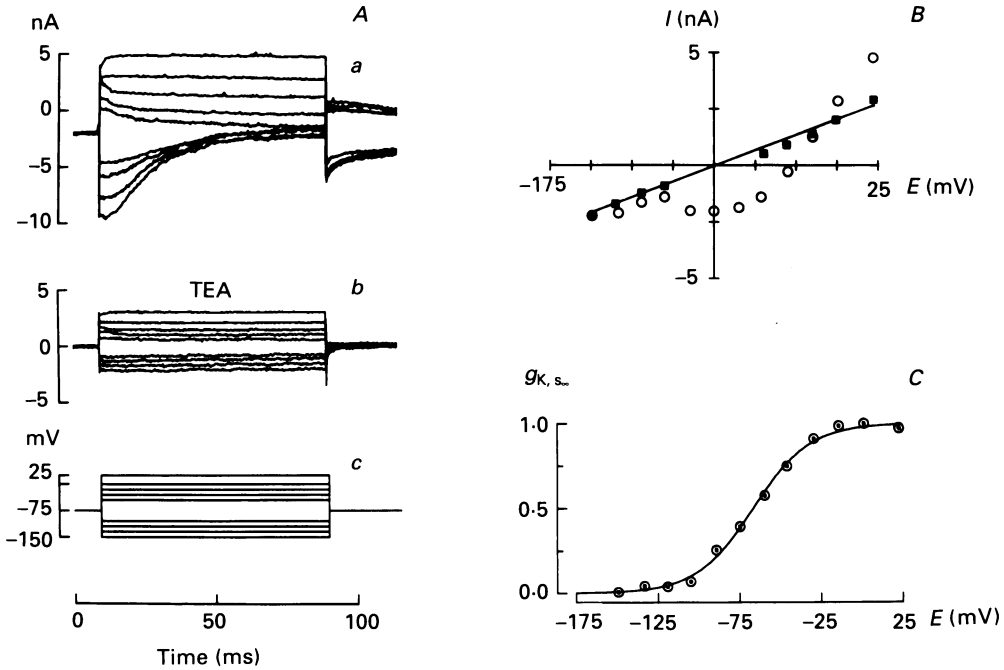

Fig. 2. K^+ currents elicited by 80 ms depolarizing and hyperpolarizing pulses of increasing amplitude. The positive pulses were from −45 to 0 mV in steps of 15 mV and one pulse to 25 mV; the negative pulses were from −105 to −150 mV in steps of 15 mV. *Aa*, measurements in isotonic KCl; *Ab*, measurements after addition of 10 mM-TEA to the isotonic KCl solution; *Ac*, pulse protocol. All measurements were made in the presence of 300 nM-TTX. Leakage and capacity currents were not subtracted. *B*, current–voltage relation of the steady-state currents in *Aa* (○) and *Ab* (■) as plotted against membrane potential. The straight line denotes the slope of the leakage current as measured in the same fibre in Ringer solution. The K^+ current (I_K) was determined from the difference between the steady-state currents and the leakage current. *C*, plot of the K^+ conductance, g_K, as calculated from the equation $g_K = I_K/(E-E_K)$ and plotted against membrane potential. The curve was calculated from the fitted parameters of a Boltzmann equation ($g_{K,s_\infty} = 1/(1-(E-E_s/k))$ with the inflexion point at $E_s = -59{\cdot}6$ mV. The steepness of the curve was given by the slope factor $k = 18{\cdot}2$ mV. The holding potential was $E_H = -75$ mV.

uppermost current trace, was 95% blocked. In four fibres, the K^+ current measured at $E = 45$ mV was 86 ± 7% blocked. However, this is a higher degree of block than that reported by Chiu & Ritchie (1981) in the rabbit and by Grissmer (1986) in the frog internode. The steady-state currents of Fig. 2*Aa* and *b* were plotted against membrane potential in Fig. 2*B*. The straight line represents the slope of the leakage current as determined by hyperpolarizing pulses in the same fibre in Ringer solution. The circles represent the amplitude of the specific K^+ current which changes direction near the theoretical K^+ equilibrium potential. The current amplitudes

measured in the presence of TEA are represented by the filled squares. Only at large positive potentials do they deviate from the line denoting the leakage current. In Fig. 2*C*, the K^+ conductance was plotted against membrane potential and a Boltzmann equation was fitted to the experimental data. The curve drawn from the fitted parameters had an inflexion point at −60 mV. Therefore, 35% of the K^+ channels were in the open state in this fibre at the holding potential of −75 mV. The same inflexion point (−59·0 ± 1·6 mV) was found in five other fibres. The same voltage dependence of the K^+ activation curve was obtained with a pulse programme identical to that shown in Fig. 2*Ac*, but with the slow K^+ conductance totally deactivated by a 500 ms hyperpolarizing pulse to −150 mV preceding each depolarizing pulse. In addition, the fast K^+ conductance was blocked by 4-AP. In our experiments, long-lasting hyperpolarizing pre-pulses or a high negative holding potential were avoided to prevent early fibre damage.

In the frog nerve, the slow K^+ conductance component characterized by Dubois (1981*a*) had almost the same kinetic parameters and potential dependence of its steady-state values as we have found in rat nerve. However, the magnitude of the steady-state K^+ conductance, g_{K,s_∞}, was significantly smaller in rat fibres (20·2 ± 1·9 nS) than in frog fibres (57 nS, see Table 1 in Dubois, 1981*a*).

Another similarity between the properties of the slow K^+ channels in the frog and rat was the observation that the amplitude and the kinetics of the K^+ tail currents depend on the duration of the depolarizing pre-pulse. Figure 3 shows the tail currents elicited after a depolarization to 0 mV for durations between 10 and 1000 ms. The amplitude of the tail currents increased approaching a steady state after a pre-pulse duration of 500 ms. The same pulse protocol was used in five fibres. The tail amplitude after a 100 ms depolarization to E_K was 64 ± 2% ($n = 5$) of the maximal amplitude obtained between 500 and 1000 ms pulse duration. The time course of the tail currents could be fitted with a single exponential. This is demonstrated in Fig. 3 where the tail current elicited after a depolarization of 1000 ms was superimposed on a single exponential obtained from a least-squares fit. After a 500 ms pulse the time constant was 168·8 ± 5·4 ms ($n = 5$). In Fig. 3*B* the time constants of the tail currents measured in the experiment of Fig. 3*A* were plotted against the duration of the preceding depolarization. Almost identical results were reported by Dubois (1981*b*).

Comparison of g_K after paranodal demyelination with g_K of the intact node

Figure 4 shows a node of Ranvier mounted in the experimental chamber before and after paranodal demyelination with 0·2% pronase. A 15 min exposure to pronase induced a pronounced paranodal destruction of the myelin, which could be stopped by washing with Ringer solution. Lysolecithin (0·2%) did not produce such large morphological changes, although its demyelinating effect in terms of increasing membrane capacity and K^+ currents was similar to that of pronase.

After paranodal demyelination, large K^+ outward and K^+ tail currents were elicited upon depolarization and repolarization, respectively. In Fig. 5, K^+ currents are compared as elicited by the same pulse protocol before and after paranodal demyelination in the same fibre. The time course of K^+ activation measured in

Ringer solution was generally slower in intact nodes of Ranvier than in demyelinated nerve fibres. Before demyelination, the time constant for I_K activation, τ_n, was $0{\cdot}57 \pm 0{\cdot}05$ ms ($n = 6$) at $E = 75$ mV. After demyelination, K^+ current activation was accelerated by a factor of 2.

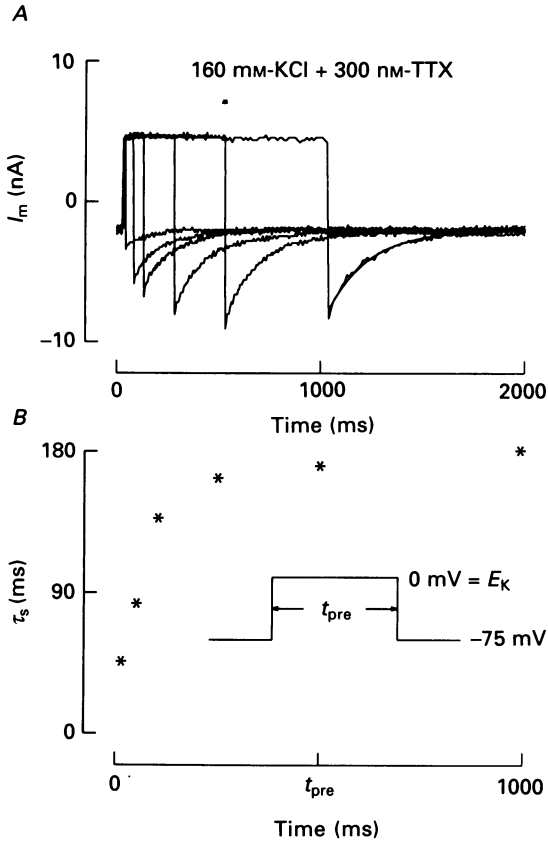

Fig. 3. *A*, the tail current time constant depends on the pre-pulse duration. The membrane was depolarized to the K^+ equilibrium potential (E_K) in isotonic KCl solution + 300 nM-TTX. K^+ tail current occurred upon repolarization to the holding potential. Least-squares fits of an exponential function to the tail currents gave the time constants. The resulting fit to the tail current elicited after the 1000 ms depolarization was superimposed on the measured tail current. The holding potential was $E_H = -77$ mV. *B*, the time constants (*) obtained from the exponential function fitted to the tail currents were plotted against the duration of the conditioning pulse.

In the intact fibre, a hyperpolarizing pulse to -150 mV was accompanied by a small and fast capacity current with a time constant within the range 0·05–0·10 ms. After demyelination, the amplitude of the fast capacity current increased and a slow capacity current component emerged which had a time constant of 3–4 ms. The amplitude of this slow capacity current represents the magnitude of the newly exposed paranodal and internodal membrane area (Chiu & Ritchie, 1981). The leakage current also increased after demyelination.

In order to minimize the artifacts induced by accumulation of K^+ ions,

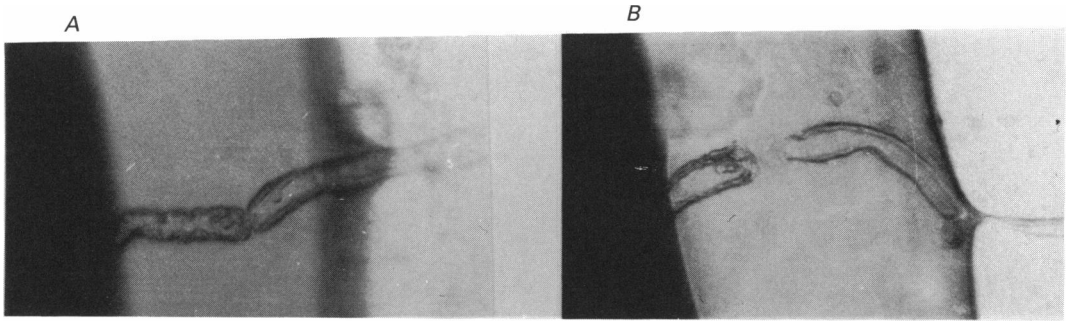

Fig. 4. Node of Ranvier of an isolated nerve fibre mounted in the experimental chamber before (*A*) and after (*B*) superfusion with 0·2% pronase for 15 min. A pronounced paranodal demyelination occurred. The photograph in *B* was taken at the end of the experiment which lasted for 90 min.

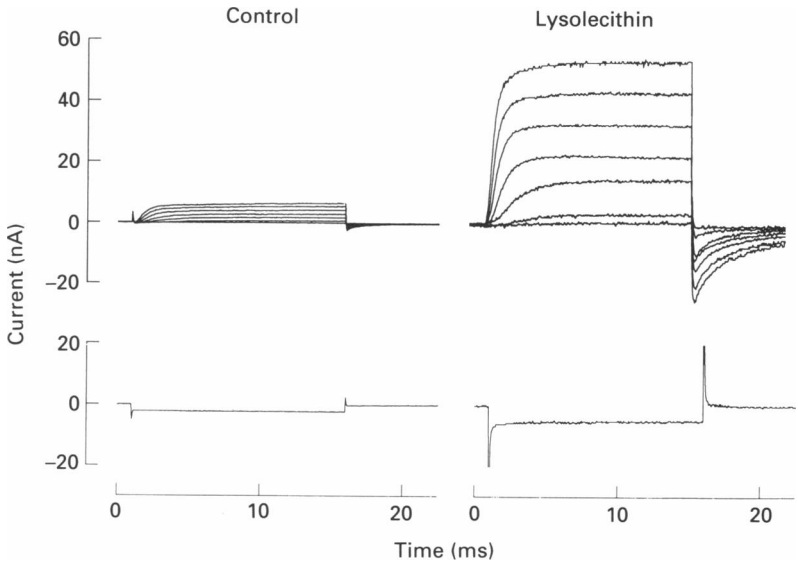

Fig. 5. K^+ currents elicited by depolarizing pulses of increasing amplitude before and after paranodal demyelination with 0·2% lysolecithin for 15 min. Pulse potentials were between −55 and 80 mV in steps of 22·5 mV. Capacity and leakage currents were elicited by the same pulse to −150 mV. External solution: Ringer solution + 300 nM-TTX. The holding potential was $E_H = -77$ mV.

measurements were performed in isotonic KCl before and after demyelination. In Fig. 6, the membrane currents are compared as recorded in two different nerve fibres. In addition to the increase in the amplitude of the K^+ outward currents, there was a change in both the amplitude and the time course of the K^+ tail currents. In intact nerve fibres, the tail currents had a small amplitude and decayed slowly. The major part of the amplitude could be fitted with only one exponential. In nine fibres, the mean contribution of the slow component to the total tail current amplitude was

$83 \pm 5\%$, indicating that nodal K^+ channels are predominantly those with slow gating kinetics. In these fibres, the total K^+ conductance was $26{\cdot}8 \pm 2{\cdot}6$ nS. After demyelination, the tail currents increased, largely due to an increase of the fast component. In the fibres shown in Fig. 6, the contribution of the fast component in the intact fibre was 20%, increasing to 80% in the demyelinated fibre. As shown below, the increase in the fast tail current component depends critically on the magnitude of the demyelinated membrane area. In seventeen nerve fibres, the time constants of the slow and fast decaying components at $E = -77$ mV were $19{\cdot}7 \pm 1{\cdot}8$ ms and $3{\cdot}7 \pm 0{\cdot}6$ ms, respectively.

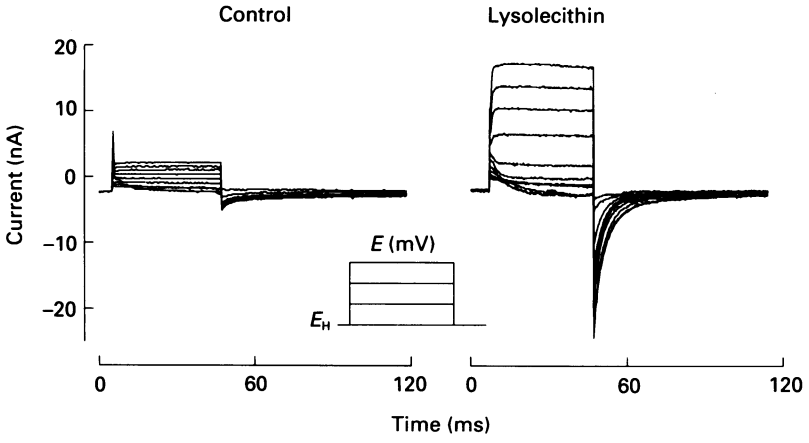

Fig. 6. K^+ currents elicited by depolarizing pulses of increasing amplitude from -60 to 75 mV in steps of 15 mV in an intact fibre and in another fibre after paranodal demyelination with 0·2% lysolecithin. $E_H = -77$ mV. External solution: isotonic KCl + 300 nM-TTX.

In the frog node of Ranvier, Dubois (1981*a*) distinguished between two fast and one slow K^+ current components. The two fast K^+ channels could be blocked selectively by 4-AP. Figure 6 (right-hand traces) as well as Fig. 7 show that the rat tail currents measured after paranodal demyelination had a similar multi-exponential time course to those measured in the intact frog node (see Fig. 1 in Dubois, 1981*a* and Fig. 4 in Grissmer, 1986). To a large degree, the fast components of these tail currents could be blocked by 1 mM-4-AP as shown in Fig. 7. The slow tail current was fitted with a single exponential which is superimposed on the tail current trace in Fig. 7. A reduction in the fast tail current component of 90% was determined from this. In four fibres, the fast K^+ tail current was blocked by $85 \pm 4\%$. In addition, the outward current, elicited by a pulse to 30 mV, was reduced, and the time course of the K^+ current activation was slowed considerably. The selective block of the fast K^+ channels by 4-AP can also be demonstrated by its ineffectiveness in blocking the steady-state inward current carried by the slow K^+ channels.

Dubois (1982) has shown that capsaicin selectively blocked one fast K^+ conductance component (f_2) in the frog. In the rat, capsaicin blocked $76 \pm 2\%$ ($n = 3$) of the fast component (Fig. 8). Assuming a similar selectivity of capsaicin in the rat as in the frog nerve fibre, the unblocked fast component should be identical to the f_1 fraction. Preliminary results, based on the evaluation of tail current measurements,

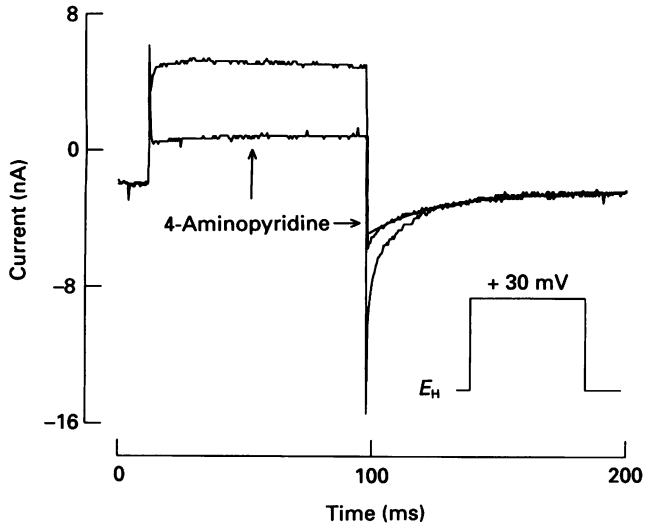

Fig. 7. K^+ tail currents elicited by a depolarizing pulse to 30 mV (see inset). The fibre had been demyelinated with 0·2% lysolecithin for 20 min. Addition of 1 mM-4-AP blocked the fast component of the K^+ tail current 90% and decreased the steady-state outward K^+ current. The steady-state inward current at the holding potential of $E_H = -77$ mV remained unaffected.

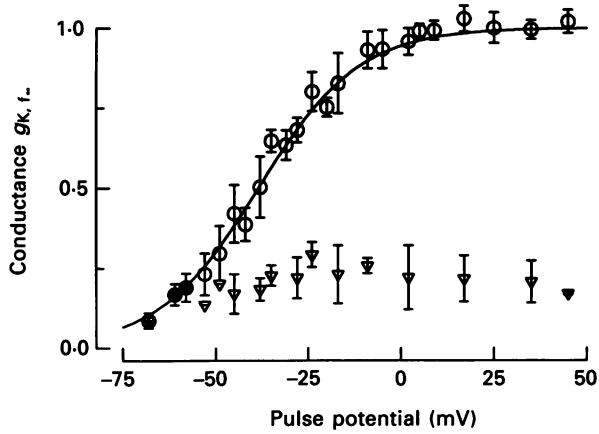

Fig. 8. Voltage dependence of the fast K^+ conductance. K^+ conductance was calculated from the K^+ tail current amplitudes after subtraction of the slow K^+ tail current component. The tail currents were recorded after pulse potentials of increasing amplitude and of 80 ms duration. The pulse potential amplitudes are given on the abscissa. Circles denote mean values of the normalized $g_{K,f}$ determined in twelve fibres. Triangles denote the mean values of fast K^+ conductance after the application of 25 μM-capsaicin as measured in three fibres. The steady-state fast g_K decreased to 24%.

indicate that in rat nerve there are also two fast components, f_1 and f_2, which are activated within a different potential range. Furthermore, Dubois (1981*a*) found that in frog sensory fibres, the relative contribution of the f_1 component is 35% whereas it is 61% in motor fibres. The small contribution of the f_1 component in rat

nerve (Fig. 8) might indicate that these fibres were sensory fibres. In our experiments, however, we had no safe criteria for distinguishing sensory and motor nerve fibres.

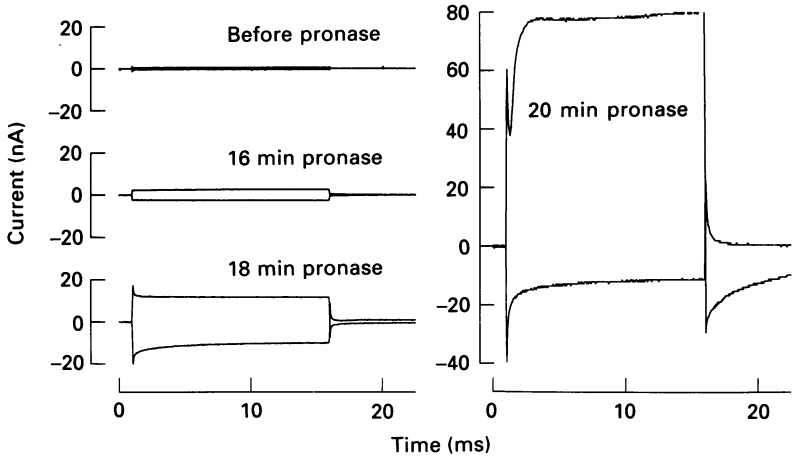

Fig. 9. The protocol of an internodal demyelination with 0·2% pronase. Symmetrical depolarizing and hyperpolarizing pulses of 100 mV were applied to the internode during continuous superfusion with 0·2% pronase in Ringer solution. Large K^+ outward currents occurred after about 16 min. At the same time, the slope of the unspecific inward current changed and a time-dependent current emerged.

Figure 9 presents the protocol of an experiment in which an internode was demyelinated (Chiu & Ritchie, 1982; Grissmer, 1986). The internode was continuously superfused with Ringer solution containing pronase or lysolecithin. At the beginning of the experiment, small leakage and capacity currents were recorded with symmetrical 100 mV pulses. These passive currents gradually increased within the first 18 min until suddenly large outward currents were elicited by the positive pulse, demonstrating the presence of K^+ channels also in the internodal membrane. From tail current measurements in isotonic KCl solution the contribution of the slow K^+ conductance component was calculated to be 15%. In addition, the leakage current and a slowly decaying capacity current increased with the exposed membrane area.

Paranodal density of fast K^+ channels

Figure 10 shows capacity currents elicited by potential steps to −150 mV in Ringer solution (on the left) and the corresponding K^+ tail current measured in KCl solution (on the right). In the upper panel, an example is shown of an intact fibre. It had a small membrane capacity of 1·5 pF and a K^+ tail current with a predominantly slow component. The middle panel shows the data of a fibre with a slightly larger membrane capacity (4·5 pF). It is clearly visible that a pronounced fast component emerged in addition to the slow component. This fibre might have been stretched during dissection. In the lower panel of Fig. 10, an example of a fibre with a large paranodal demyelination is shown; the newly exposed membrane area was equivalent to 50 pF. Its K^+ tail current was dominated by the fast tail current component.

The density of the K^+ channels was expressed as the quotient of the maximum K^+ conductance and the membrane capacity. It is plotted *versus* membrane capacity in

Fig. 11. In twenty-two fibres the maximum K^+ conductance was determined from the K^+ tail currents recorded upon repolarization to the holding potential (E_H = −77 mV) plus the fraction of the slow K^+ conductance already activated at the holding potential. The size of this fraction (35%) was taken from the activation

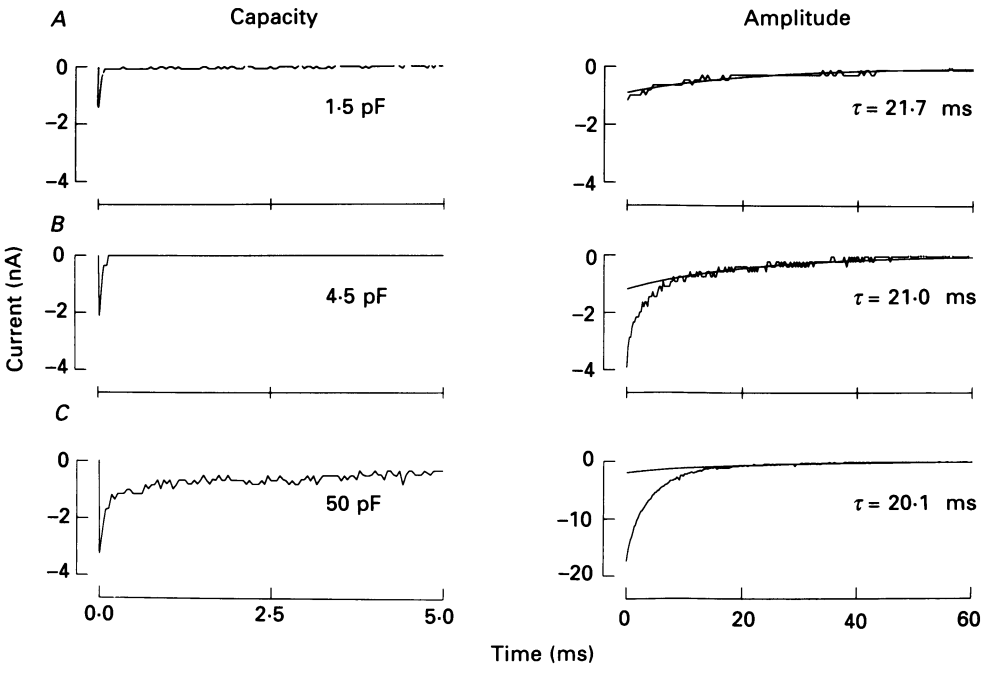

Fig. 10. Correlation of membrane capacity (on the left) and K^+ tail current amplitude (on the right). In three different fibres the membrane capacity was determined from the integral of the capacity current as elicited by a pulse to −150 mV. External solution: Ringer solution. In the same fibre the K^+ tail currents were recorded in isotonic KCl solution. The tail currents were measured upon repolarization to the holding potential of E_H = −77 mV after a 40 ms depolarization to E_K. A single exponential was fitted to the slow tail current component. *A*; intact fibre; *B*; 'stretched' fibre; *C*; fibre after 15 min demyelination with 0·2% pronase.

curve of g_{K,s_∞} (Fig. 2). The filled square represents the mean value ± S.E.M. (23·3 ± 2·2 nS pF^{-1}) of the K^+ channel density in the nine fibres with the smallest capacity currents (1·5 pF). These fibres were judged to be fibres which had not been stretched during the dissection and mounting of the fibre in the experimental chamber. Thus, they represent presumably the group of undamaged fibres. The open symbols denote individual fibres with a larger membrane capacity due to the sum of the nodal area and the newly exposed paranodal area uncovered either by stretch or demyelination. Assuming a linear relation between the increase in membrane capacity and membrane area, Fig. 11*A* shows that an increase in membrane area is correlated with a decrease in the total K^+ channel density. In fibres with an exposed membrane area corresponding to membrane capacities of between 20 and 60 pF, the channel density decreased to a constant value of 5·0 nS pF^{-1}. The same density was also calculated in a fibre with an exposed membrane area corresponding to a membrane capacity

of 180 pF. Because the fibres were very unstable after demyelination, we did not succeed in obtaining reliable measurements of the maximum K^+ conductance before and after demyelination in the same fibre. The K^+ tail current was subdivided into a fast and slow tail current component (Fig. 10). The fast and slow K^+ conductance

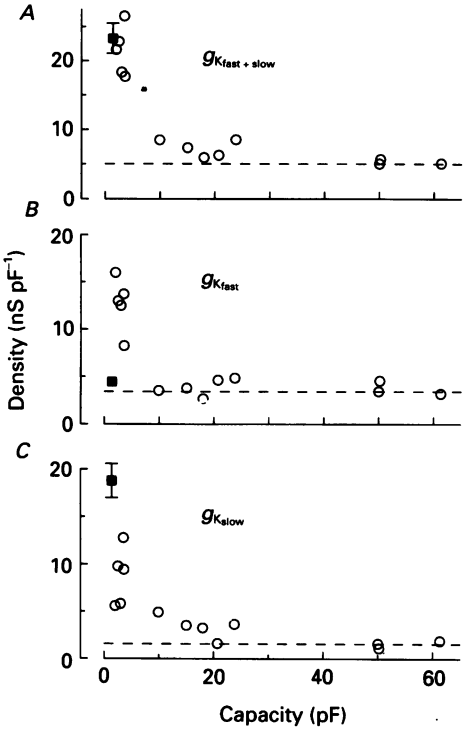

Fig. 11. Density of K^+ channels expressed as a quotient of the maximum K^+ conductance and membrane capacity plotted against membrane capacity. The total conductance (*A*) and the fast (*B*) and slow (*C*) components of the K^+ conductance were used to calculate the corresponding densities. Open symbols refer to individual fibres and filled symbols denote the mean values of nine intact fibres. Bars denote S.E.M. where larger than the symbol size.

was calculated from the amplitude of both components and duly related to the membrane capacity of the corresponding fibre. Figure 11*C* shows that the density of the slow K^+ channels was highest ($18{\cdot}8 \pm 1{\cdot}8$ nS pF^{-1}) in the intact nodes. It decreased to 1/12 in the internode with increasing membrane capacity (membrane area). By contrast, the highest density of fast K^+ channels was obtained in those nerve fibres exhibiting only a small increase in the membrane capacity (membrane area; Fig. 11*B*). It decreased from its highest value of 16·0 nS pF^{-1} to 1/4 in the node and paranode. Although the maximum density of fast and slow K^+ channels is similar for both channel types, their distribution differs. The group of intact fibres shows that the relative contribution of the slow K^+ component to the total tail amplitude was 83%. If the membrane area was only slightly increased, the contribution of the fast K^+ channels increased by a factor of 5. If larger membrane areas were exposed the density of the fast K^+ channels decreased again to the density

of the nodal membrane. This shows that the fast K^+ channels are located within a small paranodal region in the immediate vicinity of the node.

Whereas the filled symbols in Fig. 11 represent the true nodal density, the densities represented by the open symbols give the mean of the K^+ channel density of the node

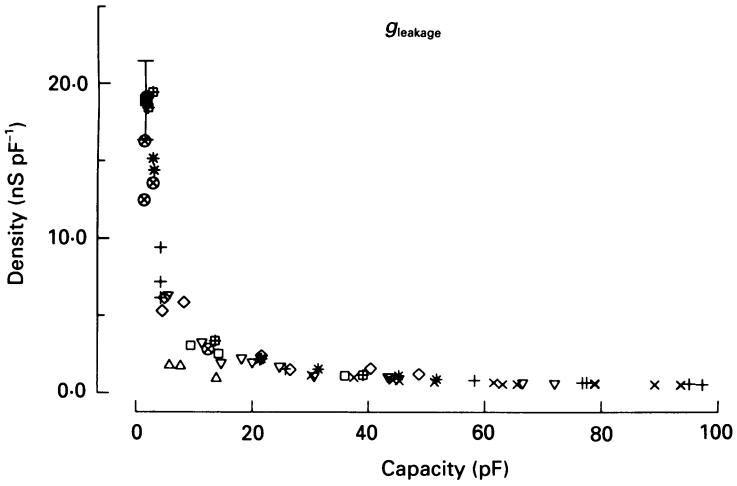

Fig. 12. Density of leakage conductance expressed as leakage conductance over membrane capacity and plotted against membrane capacity. Measurements in Ringer solution in eight fibres (different symbols) at different stages during the course of demyelination with 0·2% pronase or lysolecithin. The filled square gives the mean of seven intact fibres with very small capacity current values which had not been demyelinated. Bars denote S.E.M.

plus the newly uncovered axolemmal area. In Fig. 11*B*, for example, the peak density of the fast K^+ channels of 16 nS pF^{-1} is the mean value of the nodal and paranodal densities. This value corresponds to an exposed membrane area of 3 pF. Assuming a nodal capacity of 1·5 pF, the absolute density of the paranodal K^+ channels alone is 27·5 nS pF^{-1}; i.e. the ratio of paranodal to nodal density is 6:1. Similarly, the absolute density of slow K^+ channels decreases from the nodal value of 18·8 nS pF^{-1} to 1/31 in the internode, if an equal distribution of K^+ channels within the internode is assumed.

The leakage current was measured from the steady-state inward currents at negative pulses. In Fig. 12, the change in the leakage conductance density in nine fibres during paranodal demyelination is plotted against membrane capacity. The decrease in the leakage conductance density is similar to that of the slow K^+ channels. It decreases from its nodal value by a factor of 1/35 in the paranode and internode.

DISCUSSION

Our experiments show that in rat myelinated nerve at least two K^+ conductance components can be distinguished, suggesting the existence of two different types of K^+ channels: those with fast and those with slow gating kinetics. In addition to their different gating and pharmacology, we found that both types of K^+ channels have a different spatial distribution in the node and paranode.

Hints for the existence of slow and fast K^+ channels have earlier been reported in the nodal membrane of the frog (Schwarz & Vogel, 1971; Dubois, 1981*a*). In frog and rat myelinated nerve slow K^+ channel activation and deactivation time constants, as well as the position of the activation curve on the potential axis, are similar. The potential range of slow K^+ activation is between -100 and 0 mV with 50% activation at -60 mV. Therefore, 35% of the slow K^+ channels are in the open state at the resting potential. As in the frog, slow K^+ channels are insensitive to 4-AP but can be blocked by TEA. As a further similarity, the time constants and maximal conductances of the slow K^+ conductance component in the frog and rat as measured from tail currents depend on the duration of the depolarizing pre-pulse (Dubois, 1981*b*). This similarity is also true for the properties of fast K^+ channels. In both species the time constants and their voltage dependence are similar. They can also be blocked selectively by 4-AP. Preliminary results show that, in the rat as in the frog, there may be two different populations of fast K^+ channels which activate within different membrane potential ranges, one component being selectively blocked by capsaicin (Dubois, 1982).

In contrast to these similarities in the K^+ channel properties, the main difference between frog and rat K^+ channels is their different distribution and density along the axolemma. At least 83% of nodal K^+ conductance is provided by slow K^+ channels. They have their highest density in the nodal membrane, from which their density decreases in the paranode and internode to 1/31. By contrast, fast K^+ channels have their highest density in the paranode, forming a narrow ring of high density on either side of the nodal membrane. From the paranode fast K^+ channel density decreases in the node and internode by a factor of one-sixth. In order to calculate the density of K^+ channels, we assumed a membrane capacity of 1·5 pF for the node of Ranvier (Brismar, 1981) and 25 μm^2 for the nodal membrane area (Berthold & Rydmark, 1983). The peak density of the fast K^+ channels was correlated to a membrane capacity of 3 pF. Assuming a linear relationship between the membrane capacity and the nodal or extranodal membrane area, this increase would correlate to a membrane area of about 50 μm^2. On the basis of the data given by Berthold & Rydmark (1983) this area would cover the nodal membrane as well as parts of the paranodal membrane on each side of the node. As a result of these estimations, we assume that fast K^+ channels occur predominantly within this small paranodal region. Furthermore, we cannot exclude the possibility that fast K^+ channels are totally absent in the intact node of Ranvier and that a small fraction of fast K^+ channels is present even in very 'good' and stable preparations which have been exposed to mechanical stretch during dissection and mounting of the fibre in the experimental chamber.

The anatomical and functional organization in the node–paranode region of the rat is very complex. It comprises a highly uneven distribution of ionic channels. In addition to the high concentration of Na^+ channels, there is a high density of slow K^+ channels in the nodal membrane and fast K^+ channels in the paranode. It is not known which factors determine the heterogeneous distribution of the ionic channels in the node–paranode region. The close contact of the Schwann cell loops with the axolemma and their high mitochondria concentration may characterize the paranode as a location for a functional glia–axon interaction. The transfer of ionic channel

proteins to the axolemma might take place within this region. This hypothesis is supported by the presence of 4-AP and TEA-sensitive K^+ channels in cultured Schwann cells (Shrager, Chiu & Ritchie, 1985; Howe & Ritchie, 1988) with the same properties as those found in the node and paranode. The general possibility of transmembrane protein transfer from glia to axon was shown by Lasek & Tytell (1981) in squid.

Several authors (Brismar, 1980; Binah & Palti, 1981; Brismar & Schwarz, 1985) have hinted at the existence of nodal K^+ channels in rat nerve which are in the open state at the normal resting potential due to the position of the activation curve with 50% activation near the resting potential. Our results support these observations and indicate that the K^+ conductance properties described in these papers can be attributed to the properties of slow K^+ channels described in our present work. In the frog, nodal K^+ conductance is larger (319 nS) than in the rat (35 nS). Furthermore, there is a difference in the relative contribution of slow K^+ conductance to total K^+ conductance. The proportion of slow K^+ channels is 17% (57·4 nS) in the frog and 83% (20·2 nS) in the rat. Therefore the slow K^+ conductance is smaller by a factor of 2·8 in the rat compared with that of the frog. However, the main difference is in the contribution of the fast K^+ channels. This contribution is smaller by a factor of 1/39 (261·6 nS in the frog (Dubois, 1981*a*) compared with 6·7 nS in the rat).

In view of the minimal effects of TEA (Schwarz & Eikhof, 1987) and 4-AP (Sherrat *et al.* 1980) on action potential duration in adult nerve fibres, slow and fast K^+ channels are not involved in action potential electrogenesis. Nevertheless, a functional significance of these two K^+ channel types is illustrated by the model for saltatory conduction suggested by Barrett & Barrett (1982). In this model, a significant portion of the current underlying the propagated action potential is directed backwards through the longitudinal resistance pathway of the periaxonal space and the paranodal region. Microelectrode studies in single mammalian nerve fibres (Baker *et al.* 1987) demonstrated that TEA reduces accommodation and 4-AP induces burst-like behaviour (Koksis & Waxman, 1987). The role of slow K^+ channels in spike frequency adaptation has already been shown by Krylov & Markowsky (1978) in frog nerve. Due to their paranodal location, fast 4-AP-sensitive K^+ channels are activated by the current induced by the propagated action potential flowing backwards through the periaxonal pathway. In this way, they may prevent excitation by the fast re-entry of this current. This mechanism could explain the observation that block of the fast K^+ channels leads to burst-like behaviour (Baker *et al.* 1987; Koksis & Waxman, 1987).

In the internode, the low density of fast and slow K^+ channels as well as the small leakage conductance contribute to the high input resistance of the internodal membrane reducing the transmembrane current flow. The open fraction of the internodal slow K^+ channels may be responsible for the internodal resting potential important for maintaining the nodal resting potential (Chiu & Ritchie, 1984).

We thank Professor B. Bromm for continuous support throughout this work and Dr Christiane Bauer and Professor H. Meves for critically reading the manuscript and for many helpful suggestions. This work was supported by a grant of the Deutsche Forschungsgemeinschaft to J.R.S. (Schw 292/3-2).

REFERENCES

BAKER, M., BOSTOCK, H., GRAFE, P. & MARTIUS, P. (1987). Function and distribution of three types of rectifying channel in rat spinal root myelinated axons. *Journal of Physiology* **383**, 45–67.

BARRETT, E. F. & BARRETT, J. N. (1982). Intracellular recordings from vertebrate myelinated axons: mechanism of the depolarizing after-potential. *Journal of Physiology* **323**, 117–144.

BERTHOLD, C.-H. & RYDMARK, M. (1983). Anatomy of the paranode–node–paranode region in the cat. *Experientia* **39**, 964–976.

BINAH, O. & PALTI, Y. (1981). Potassium channels in the nodal membrane of rat myelinated fibres. *Nature* **290**, 598–600.

BRISMAR, T. (1979). Potential clamp experiments on myelinated nerve fibres from alloxan diabetic rats. *Acta physiologica scandinavica* **105**, 384–386.

BRISMAR, T. (1980). Potential clamp analysis of membrane currents in rat myelinated nerve fibres. *Journal of Physiology* **298**, 171–184.

BRISMAR, T. (1981). Electrical properties of isolated demyelinated rat nerve fibres. *Acta physiologica scandinavica* **113**, 161–166.

BRISMAR, T. & SCHWARZ, J. R. (1985). Potassium permeability in rat myelinated nerve fibres. *Acta physiologica scandinavica* **124**, 141–148.

CHIU, S. Y. & RITCHIE, J. M. (1981). Evidence for the presence of potassium channels in the paranodal region of acutely demyelinated mammalian single nerve fibres. *Journal of Physiology* **313**, 415–437.

CHIU, S. Y. & RITCHIE, J. M. (1982). Evidence for the presence of potassium channels in the internode of frog myelinated nerve fibres. *Journal of Physiology* **322**, 485–501.

CHIU, S. Y. & RITCHIE, J. M. (1984). On the physiological role of internodal potassium channels and the security of conduction in myelinated nerve fibres. *Proceedings of the Royal Society* B **220**, 415–422.

CHIU, S. Y., RITCHIE, J. M., ROGART, R. B. & STAGG, D. (1979). A quantitative description of membrane currents in rabbit myelinated nerve. *Journal of Physiology* **292**, 149–166.

CHIU, S. Y. & SCHWARZ, W. (1987). Sodium and potassium currents in acutely demyelinated internodes of rabbit sciatic nerves. *Journal of Physiology* **391**, 631–649.

DUBOIS, J. M. (1981*a*). Evidence for the existence of three types of potassium channels in the frog Ranvier node membrane. *Journal of Physiology* **318**, 297–316.

DUBOIS, J. M. (1981*b*). Properties of the slow K^+ current of the nodal membrane. *Journal de Physiologie* **77**, 1129–1134.

DUBOIS, J. M. (1982). Capsaicin blocks one class of K^+ channels in the frog node of Ranvier. *Brain Research* **245**, 372–375.

GRISSMER, S. (1986). Properties of potassium and sodium channels in frog internode. *Journal of Physiology* **381**, 119–134.

HOWE, J. R. & RITCHIE, J. M. (1988). Two types of potassium current in rabbit cultured Schwann cells. *Proceedings of the Royal Society* B **235**, 19–27.

KOKSIS, J. D. & WAXMAN, S. G. (1987). Ionic channel organization of normal and regenerating mammalian axons. In *Progress in Brain Research*, vol. 71, ed. SEIL, F. J., HERBERT, E. & CARLSON, B. M., pp. 89–101. Amsterdam: Elsevier.

KOKSIS, J. D., WAXMAN, S. G., HILDEBRAND, C. & RUIZ, J. A. (1982). Regenerating mammalian nerve fibres: changes in action potential waveform and firing characteristics following blockage of K conductance. *Proceedings of the Royal Society* B **217**, 77–87.

KRYLOV, B. V. & MARKOVSKY, V. S. (1978). Spike frequency adaptation in amphibian sensory fibres is probably due to slow K channels. *Nature* **275**, 549–551.

LASEK, R. J. & TYTELL, M. A. (1981). Macromolecular transfer from glia to axon. *Journal of Experimental Biology* **95**, 153–165.

NEUMCKE, B., SCHWARZ, J. R. & STÄMPFLI, R. (1987). A comparison of sodium currents in rat and frog myelinated nerve: normal and modified sodium inactivation. *Journal of Physiology* **382**, 175–191.

NEUMCKE, B. & STÄMPFLI, R. (1982). Sodium currents and sodium-dependent fluctuations in rat myelinated nerve fibres. *Journal of Physiology* **329**, 163–184.

NONNER, W. (1969). A new voltage clamp method for Ranvier nodes. *Pflügers Archiv* **309**, 176–192.

SCHWARZ, J. R. & EIKHOF, G. (1987). Na currents and action potentials in rat myelinated nerve fibres at 20 and 37 °C. *Pflügers Archiv* **409**, 569–577.

SCHWARZ, J. R. & RÖPER, J. (1988). Nodal and paranodal K channels in myelinated rat nerve. *European Journal of Neuroscience*, suppl. 89.2.

SCHWARZ, J. R. & VOGEL, W. (1971). Potassium inactivation in single myelinated nerve fibres of *Xenopus laevis*. *Pflügers Archiv* **330**, 61–73.

SHERRATT, R. M., BOSTOCK, H. & SEARS, T. A. (1980). Effects of 4-aminopyridine on normal and demyelinated nerve fibres. *Nature* **283**, 570–572.

SHRAGER, P., CHIU, S. Y. & RITCHIE, J. M. (1985). Voltage-dependent Na and K channels in mammalian cultured Schwann cells. *Proceedings of the National Academy of Sciences of the USA* **82**, 948–952.

STÄMPFLI, R. & HILLE, B. (1976). Electrophysiology of the peripheral nerve. In *Handbook of Frog Neurobiology*, ed. LLINÀS, R. & PRECHT, W., pp. 3–32. Berlin, Heidelberg, New York: Springer–Verlag.